A modal-spectral model for flanking transmissions

J. Poblet-Puig*[1]

[1]Laboratori de Càlcul Numèric, E.T.S. d'Enginyers de Camins, Canals i Ports de Barcelona, Universitat Politècnica de Catalunya

August 7, 2016

Abstract

A model for the prediction of direct and indirect (flanking) sound transmissions is presented. It can be applied to geometries with extrusion symmetry. The structures are modelled with spectral finite elements. The acoustic domains are described by means of a modal expansion of the pressure field and must be cuboid-shaped. These reasonable simplifications in the geometry allow the use of more efficient numerical methods. Consequently the coupled vibroacoustic problem in structures such as junctions is efficiently solved. The vibration reduction index of T-junctions with acoustic excitation and with point force excitation is compared. The differences due to the excitation type obey quite general trends that could be taken into account by prediction formulas. However, they are smaller than other uncertainties not considered in practice. The model is also used to check if the sound transmissions of a fully vibroacoustic problem involving several flanking paths can be reproduced by superposition of independent paths. There exist some differences caused by the interaction between paths, which are more important at low frequencies.

1 Introduction

Predictions of the direct and indirect (flanking) sound transmission are important in order to make proper acoustic designs of buildings, ships or train wagons. But the simulations done by means of the finite element method (FEM), the boundary element method (BEM) or other deterministic techniques based on space discretisation are often time consuming and computationally expensive due to several reasons: the need to cover a wide frequency range of audible noise, the mandatory use of smaller elements when frequency increases, the large dimensions of the physical domains to be considered or the big number of situations to be analysed in order to understand the problem and provide practical design rules.

*correspondence: UPC, Campus Nord B1, Jordi Girona 1, E-08034 Barcelona, Spain, e-mail: jordi.poblet@upc.edu

This is especially critical in the field of building acoustics where numerical simulations are often restricted to the low-frequency range and/or two-dimensional problems. Very often the interest is focused to describe the behaviour of a single component (i.e. sound transmission through a single wall, vibration response of a junction). However, the problem of flanking transmission is global in the sense that it affects several acoustic domains and more or less complex and big structures. It causes computational requirements to be larger and quite often unaffordable.

The use of semi-analytical models or statistical techniques such as Statistical Energy Analysis (SEA) [1] which hypotheses are valid only at high frequencies is very common in order to complement and cover the whole frequency range of interest. An important example is the global model proposed in the EN-12354 [2]. It accounts for all transmission types (direct and flanking) and it is based on a first order SEA formulation [3, 4]. The main input required by the model in order to deal with flanking transmissions is the vibration reduction index. Recent researches try to provide practical design data by studying the structural junctions in the laboratory [5, 6], by means of finite element models [7], using wave approach [8], or wave-based or spectral finite elements (SFEM) [9, 10, 11]. All of them are restricted to the study of vibration transmissions through the junction.

In the present work, a model is formulated and implemented in a computer software in order to complement these simulations but including now the acoustic part of the problem (i.e. rooms that are separated by the junction). The starting point is the model developed in [9]. The vibroacoustic problem to be analysed is restricted to geometries with extrusion symmetry where the acoustic domains are cuboid-shaped. This allows the attainment of a computationally efficient formulation. It uses spectral finite elements [12, 13, 14] for the structure part and expand the pressure field in the acoustic domains in terms of the analytical expression of the eigenfunctions. All these keep the model general enough to deal with a great variety of junctions and structures. The results obtained are fully equivalent to a FEM simulation. So, they are valid for all frequencies and are not subjected to hypotheses of physical nature such as the ones required by SEA (they are only satisfied when the frequency is high enough in order to guarantee large modal density of each subsystem among other aspects). Since the model is oriented to reduce the computational costs of FEM or BEM for problems satisfying the restrictions mentioned above, a larger frequency range can be simulated. Moreover, an ensemble of situations can be considered as an attempt to reproduce the uncertainty and statistical nature of the physical phenomenon at mid frequencies where the modal overlap starts to be important.

The contributions of the research are:

- Formulation, implementation and testing of a deterministic model accounting for extrusion symmetry vibroacoustic problems in a wide frequency range with smaller computation costs than other element-based methods

- Coupling of the SFEM for shells with the modal expansion of cuboid acoustic domains.

- Computation of the vibration reduction indices for heavy junctions with acoustic excitation (instead of mechanical or point forces)

Both components of the model presented here: the use of modal analysis to describe the pressure field in acoustic cavities or rooms and the derivation of spectral or wave-based elements are not new. However, to the best of the author knowledge a model combining these techniques and its application to the problem of flanking transmissions has not been presented before.

Analytical modal expansion of the pressure field in cavities is a good option when: *i)*the shape of the domains to be studied is simple but the dimensions large; *ii)*the computational costs must be optimised at maximum; *iii)*it is important to cover a wide frequency range to gain knowledge on the physics of the problem and *iv)*the coupling is weak enough in order to consider the *in vacuo* modes of each sub-domain of the problem. This technique, recently reviewed in [15], has been considered in the study of a cuboid-shaped cavity coupled with a rectangular plate [16, 17, 18], the sound transmission between cuboid-shaped rooms separated by: a single wall [19, 20, 21, 22, 23, 24, 25, 26, 27], a double wall [28, 29], cavities of double walls [30], slits and holes [31] or the transmissions between continuous plates coupled to rooms [32]. Other models combine a modal description in one plane with a description in function of plane waves propagating in positive and negative direction normal to the modal plane which helps in order to impose the continuity of normal velocity. See for example [33] with an application to the sound transmission through cross sections that can be composed of an aperture and flexible structures, [23, 34, 35] for sound transmission problems, or [36] where in a problem of the sound transmission through a single wall, the direction orthogonal to the wall is infinite.

The most common option is to consider normal modes (case of rigid walls or null normal velocity in all the boundaries), see the general theory in [37]. Their analytical expression is simple, they have interesting orthogonality properties and provide good approximation when the absorption or damping is not very high. This is the option chosen here. However, other options better adapted to satisfy the absorbing (Robin) boundary conditions [38] or the pressure field around a point source [39] exist.

The dynamic stiffness methods and the SFEM are also a good option to deal with the study of structural vibration in a wide frequency range. They have been used, among others, to predict the vibration behaviour of structures composed of panels [40]. Most of these methods require the assumption of some geometry simplification. But recent formulations try to extend their use to more general structures, for example composed of rectangular plates [41, 42, 43].

The manuscript is organised as follows. The model is presented in Section 2. The interest is focused on the way how the SFEM and the modal expansion of the acoustic domains are coupled. The numerical examples are shown in Section 3, including a comparison with the finite strip method (FSM) and the parametric analysis of the T-shaped junction. The discussion of the results and possible future improvements is done in Section 4 and the paper is finished with the conclusions of Section 5.

2 Method and theory

2.1 Model overview

The goal is to formulate a deterministic model that could deal with vibroacoustic problems of quite large dimensions (which is often the situation in building acoustics), in a wide frequency range, with reduced computational costs and considering structures a bit more complex than a single or double wall. The price to satisfy this requirements is to assume some simplifications in geometry and boundary conditions in order to use numerical techniques less generic but more efficient than FEM or BEM. SFEM allows the description of the structure with few nodes and elements. The modal expansion of the acoustic domains provides a quite accurate estimation of the pressure field with few modes (much less than nodes in the equivalent FEM discretisation).

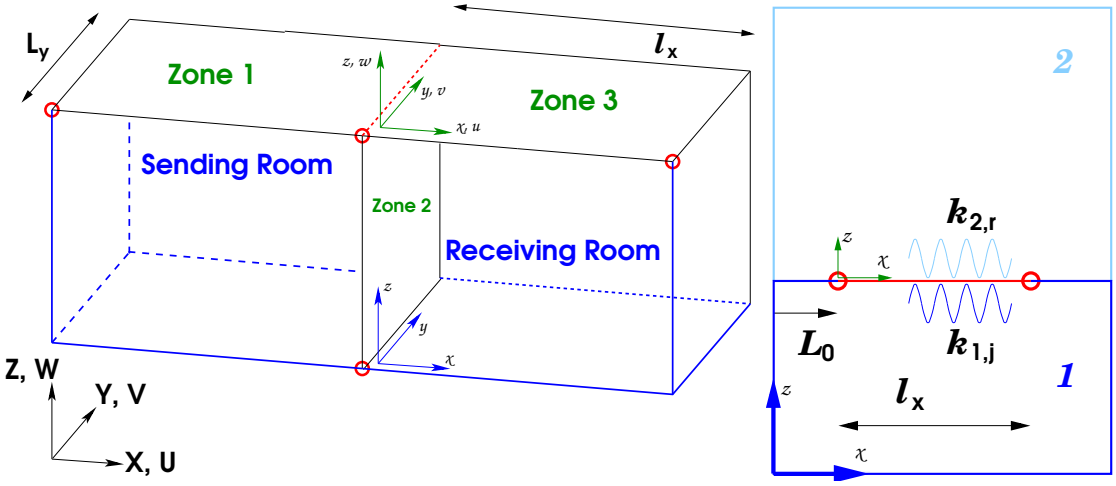

(a) (b)

Figure 1: Sketches and notation: (a)Model of a T-shaped junction with three spectral finite elements. Red circles indicate the used nodes (4). X, Y, Z are the global coordinates with displacements U, V, W. The length in the extrusion direction is L_y. The spectral finite element with dimensions $l_x \times L_y$ has local coordinates x, y, z with local displacements u, v, w; (b)A single spectral element separating two acoustic domains, one at each side.

The problem is solved in the frequency-domain (steady harmonic linear elastic structures and acoustic fluids). A pressure-displacement formulation is used. The interaction between the acoustic fluid and the structure is considered only in the normal direction (as usual, the tangential friction is neglected). The implementation allows the control of the coupling and it can be decided if the contact surfaces between fluid and structure interact or not. If nothing is specified, fully coupled situations are considered (all the coincident surfaces allow fluid-structure interaction in all senses, without *a priori* hypotheses).

The geometries must have extrusion symmetry due to the spectral elements considered and the shape of the acoustic domains. An example is the T-shaped junction

of Fig. 1(a) (with extrusion symmetry along the $Y \equiv y$ direction). All the structures analysed are supported on a roller at the planes $Y = 0$ and $Y = L_y$ where the blocked displacements are $U = 0$ and $W = 0$ (V is free there). It must be noted that diffusors have not been included in the model. They are required by the standard [44] but would complicate the formulation. The effect of the diffuse field is reproduced by providing averaged results in the third-octave frequency bands. Moreover, when the output is pretended to be more general, the results obtained with different problem dimensions are averaged.

The variation along the Y direction is described by means of trigonometric functions (sine series are used here). It affects not only the pressure description but also all other room variables: excitations, wall absorption, etc. This leads to an important advantage of the method: each contribution n is solved independently from the others. On the contrary, the use of sine series in the Y direction forces the type of boundary conditions to be considered at $Y = 0$ and $Y = L_y$ in both the structure and the acoustic domains. For the structure, it implies that $U = W = 0$, which is quite usual. However, for the acoustic domains it implies the assumption of the non very realistic condition of zero pressure at walls. With the positive aspect that the acoustic intensity through the surfaces at $Y = 0$ and $Y = L_y$, which is required to calculate the sound reduction index, is known (null). This enforcing of boundary condition in the fluid domains is probably the most important drawback of the model but a required assumption in order to simplify the formulation and reduce the computational costs. These types of assumptions that sacrifice realism for the sake of better efficiency are quite usual in vibroacoustic models. Unfortunately it is a cost to pay in order to derive less complex formulations and adapt the computational costs to the available resources. The latter is essential, otherwise the computation limitations can lead to more undesired consequences that could be important for the final results (such as the derivation of wrong conclusions in the mid frequency range due to the small number of problem frequencies to be averaged). The physical implications will be shown latter in Section 4. All other boundary conditions in the other zones can be imposed as it is done in spectral elements and modal expansions. In the remainder of the section the formulation is presented for each harmonic 'n' but the subscript is omitted for clarity (except for the parameter $\xi_n = n\pi/L_y$). In order to obtain the final result a combination of each uncoupled component 'n' must be done.

The structural elements are shells. The in-plane behaviour (local displacements u, v) is considered as described in [9]. It is decoupled from the out-of-plane displacements (w). The formulation exposed here focuses the interest on the out-of-plane displacements (bending) and the interaction with the fluid domains. The remainder of the section explains how a spectral finite element is coupled with cuboid-shaped fluid domains (see for example the single element of Fig. 1(b)). This must be, afterwards, combined with the in-plane part of the structural element, a global assembly process (that is standard) and the inclusion in the global solution of the coupled problem.

2.2 Fluid→structure interaction: acoustic loading of the structure

The out-of-plane displacements must be of the form

$$w(x,y) = \hat{w}(x)\sin(\frac{n\pi}{L_y}y) \qquad (x,y) \in [0,l_x]\times[0,L_y] \tag{1}$$

where x, y are the local coordinates in the element plane, l_x is the element length in the x direction, L_y is the problem/element length in $y-$direction. Note that due to the extrusion symmetry $\hat{w}$ is always parallel to the $X-Z$ plane (the 'hat' is reserved here for the variables reduced to the $X-Z$ plane, when the treatment of the $y-$direction has been separated).

The out-of-plane displacements are governed by the thin plate equation

$$\frac{\partial^4 w}{\partial x^4} + \frac{\partial^4 w}{\partial x^2 \partial y^2} + \frac{\partial^4 w}{\partial y^4} - \beta^2 w = -\frac{q(x,y)}{D} \tag{2}$$

with

$$\beta = \sqrt{\frac{\rho_v t\omega^2}{D}} \quad D = \frac{t^3 E(1+\mathrm{i}\eta)}{12(1-\nu^2)}. \tag{3}$$

Here ρ_v is the volumetric density of the shell, t its thickness, ν the Poisson's ratio, E the Young's modulus, η the hysteretic damping coefficient, $\omega = 2\pi f$ the pulsation of the problem and $\mathrm{i} = \sqrt{-1}$ the imaginary unit. $q(x,y)$ is the external load per unit surface in the direction of w. If it can be expressed as

$$q(x,y) = \hat{q}(x)\sin(\frac{n\pi}{L_y}y) \tag{4}$$

then the formulation of the element is one-dimensional instead of two-dimensional and Eq. (2) can be rewritten as

$$\frac{d^4\hat{w}}{dx^4} - 2\xi_n^2\frac{d^2\hat{w}}{dx^2} + \left(\xi_n^4 - \beta^2\right)\hat{w} = -\frac{\hat{q}}{D} \tag{5}$$

which is an Ordinary Differential Equation (ODE) (instead of a Partial Differential Equation, PDE) on x. It allows solutions of the form:

$$\hat{w} = \hat{w}^H + \hat{w}^P \tag{6}$$

accounting for the homogeneous (H) and particular (P) parts. The roots of the characteristic polynomial are $\pm\sqrt{\xi_n^2 - \beta}$ and $\pm\sqrt{\xi_n^2 + \beta}$. So, the homogeneous solution is of the form

$$\hat{w}^H(x) = A_1 e^{-\mathrm{i}k_1 x} + B_1 e^{-\mathrm{i}k_2 x} + C_1 e^{-\mathrm{i}k_1(l_x - x)} + D_1 e^{-\mathrm{i}k_2(l_x - x)} = \mathbf{N}^{SEM}\cdot\mathbf{A}^T \tag{7}$$

with k_1 and k_2

$$k_1 = \sqrt{\beta - \xi_n^2} \qquad k_2 = -\mathrm{i}\sqrt{\beta + \xi_n^2}; \tag{8}$$

and

$$\mathbf{N}^{SEM} = \left[e^{-\mathrm{i}k_1 x}, e^{-\mathrm{i}k_2 x}, e^{-\mathrm{i}k_1(l_x - x)}, e^{-\mathrm{i}k_2(l_x - x)}\right] \qquad \mathbf{A} = [A_1, B_1, C_1, D_1] \tag{9}$$

The key here is how to introduce the particular solution in the formulation of the spectral element with minor modifications. Similar procedures can be found in [45] where random excitation is introduced along the elements of a beam framework, in [46] where the axial and bending load in beam elements is described by means of finite element discretisation type or in [47] where spectral elements for rectangular plates subjected to turbulence excitation are formulated or [48] with an application for pipes.

In the current model the excitations caused by the acoustic pressure on the contour of the cuboid-shaped domains are of the form

$$\hat{q}\,(x) = \sum_{s}^{1\ or\ 2} \sigma_s \sum_{j} P_{s,j} \cos\left(\kappa_{s,j} x + \varphi_{s,j}\right) \tag{10}$$

with $\varphi_{s,j} = L_0 \kappa_{s,j}$ according to Fig. 1(b) and $\kappa_{s,j}$ the wavenumber of the imposed pressure on the s-side of the element. $\sigma_s = \pm 1$ accounts for the sign criterion related with the local coordinates of the spectral element. In Fig. 1(b), $\sigma_1 = 1$ and $\sigma_2 = -1$. $P_{s,j}$ is a constant that will be related latter with the modal contribution of the pressure field.

With this excitation, the particular solution of the ODE in Eq. (5) is

$$\hat{w}^P\,(x) = \frac{1}{D} \sum_{s}^{1\ or\ 2} \sum_{j} \hat{w}^P_{s,j}\,(x) = \frac{1}{D} \sum_{s}^{1\ or\ 2} \sigma_s \sum_{j} \Psi_{s,j} P_{s,j} \cos\left(\kappa_{s,j} x + \varphi_{s,j}\right) \tag{11}$$

with

$$\Psi_{s,j} = \frac{1}{(\xi_n^4 - \beta^2) + 2\kappa_{s,j}^2 \xi_n^2 + \kappa_{s,j}^4} \tag{12}$$

A bending dynamic stiffness matrix for the spectral element can be obtained by means of two steps: *i)* Express the boundary strengths (bending moment and shear force) in terms of the constants A_1, B_1, C_1 and D_1 and the parameters of the particular solution; *ii)* Express the constants A_1, B_1, C_1 and D_1 and the parameters of the particular solution in terms of the nodal displacements and rotations.

The forces and moments per unit length at the nodes of the element are expressed as

$$F_z(x=0,y) = D\left(\left.\frac{d^3 w}{dx^3}\right|_{x=0} - \xi_n^2 (2-\nu) \left.\frac{dw}{dx}\right|_{x=0} \right) \tag{13}$$

$$M(x=0,y) = D\left(-\left.\frac{d^2 w}{dx^2}\right|_{x=0} + \xi_n^2 \nu\, w|_{x=0} \right) \tag{14}$$

$$F_z(x=l_x,y) = D\left(-\left.\frac{d^3 w}{dx^3}\right|_{x=l_x} + \xi_n^2 (2-\nu) \left.\frac{dw}{dx}\right|_{x=l_x} \right) \tag{15}$$

$$M(x=l_x,y) = D\left(\left.\frac{d^2 w}{dx^2}\right|_{x=l_x} - \xi_n^2 \nu\, w|_{x=l_x} \right) \tag{16}$$

Using the displacement defined in Eq. (6), the forces can be written as

$$\mathbf{f}_e = \begin{bmatrix} F_z(x=0,y) \\ M(x=0,y) \\ F_z(x=l_x,y) \\ M(x=l_x,y) \end{bmatrix} = \mathbf{B}_e \begin{bmatrix} A_1 \\ B_1 \\ C_1 \\ D_1 \end{bmatrix} + \sum_{s}^{1\ or\ 2} \sigma_s \sum_{j} \Psi_{s,j} P_{s,j} \mathbf{F}^p_{s,j} \tag{17}$$

with $\mathbf{B}_e$ detailed in A and the contribution of the particular solution to the nodal forces

$$\mathbf{F}^p_{s,j} = \begin{bmatrix} \left(\xi_n^2(2-\nu)+\kappa_{s,j}^2\right)\kappa_{s,j}\sin(\varphi_{s,j}) \\ \left(\xi_n^2\nu+\kappa_{s,j}^2\right)\cos(\varphi_{s,j}) \\ \left(-\xi_n^2(2-\nu)-\kappa_{s,j}^2\right)\kappa_{s,j}\sin(\kappa_{s,j}l_x+\varphi_{s,j}) \\ \left(-\xi_n^2\nu-\kappa_{s,j}^2\right)\cos(\kappa_{s,j}l_x+\varphi_{s,j}) \end{bmatrix} \tag{18}$$

Next step is to express the nodal displacements and rotations in terms of the constants A_1, B_1, C_1 and D_1, and the parameters related with the particular solution. A 4×4 system of linear equations is obtained by the evaluation of Eq. (6) at $x=0$ and $x=l_x$

$$\mathbf{u}_e = \begin{bmatrix} w|_{x=0} \\ \frac{dw}{dx}\big|_{x=0} \\ w|_{x=l_x} \\ \frac{dw}{dx}\big|_{x=l_x} \end{bmatrix} = \mathbf{S}\begin{bmatrix} A_1 \\ B_1 \\ C_1 \\ D_1 \end{bmatrix} + \frac{1}{D}\sum_{s}^{1\ or\ 2}\sigma_s\sum_j \Psi_{s,j}P_{s,j}\underbrace{\begin{bmatrix} \cos(\varphi_{s,j}) \\ -\kappa_{s,j}\sin(\varphi_{s,j}) \\ \cos(\kappa_{s,j}l_x+\varphi_{s,j}) \\ -\kappa\sin(\kappa_{s,j}l_x+\varphi_{s,j}) \end{bmatrix}}_{\mathbf{u}^p_{s,j}} \tag{19}$$

$\mathbf{S}$, also detailed in A, is a small matrix that can be inverted in order to compute the bending dynamic stiffness matrix $\mathbf{K}_e^{bending}$ such that

$$\mathbf{K}_e^{bending} = \mathbf{B}_e\mathbf{S}^{-1} \tag{20}$$

and finally the matrix formulation at element level that accounts for possible coupling is

$$\mathbf{K}_e^{bending}\mathbf{u}_e + \sum_{s}^{1\ or\ 2}\sum_j \underbrace{\sigma_s\Psi_{s,j}\left(\mathbf{F}^p_{s,j}-\frac{1}{D}\mathbf{K}_e^{bending}\mathbf{u}^p_{s,j}\right)}_{(\mathbf{C}^s_{FS})_{\cdot,j}}P_{s,j} = \mathbf{f}_e \tag{21}$$

with $\mathbf{C}^s_{FS}$ the coupling matrix that accounts for the coupling force applied to the s side of the spectral element and $\mathbf{f}_e$ is the vector of nodal forces defined in Eq. (17).

2.3 Structure→fluid interaction: imposed velocity on the fluid contour

The weak form used in [31] for the acoustic domains is considered. It must be adapted in order to account for the coupling with the spectral element. Moreover, the modes of the cuboid must be modified in order to have the same trigonometric description of the pressure field in the extrusion direction as the shell spectral element. So, the pressure field is expanded in terms of modes as

$$p(x,y,z) = \mathcal{Y}_n(y)\sum_{j=1}^{n_{modes}} p_j\psi_j(x,z) \tag{22}$$

with

$$\psi_j = \cos\left(\frac{n_{xj}\pi}{l_x}x\right)\cos\left(\frac{n_{zj}\pi}{l_z}z\right) \qquad n_{xj}, n_{zj} = 0,1,2,\ldots,j,\ldots \tag{23}$$

and

$$\mathcal{Y}_n\left(y\right) = \sin\left(n\pi/L_y y\right) \tag{24}$$

p_j is the contribution of mode j.

The weak form can be written as

$$\begin{aligned}\left(k^2 - k_i^2\right)\int_\Omega \upsilon p \; d\Omega - \mathrm{i}\rho\omega\int_{\Gamma_R} A\;\upsilon p\; d\Gamma + \rho\omega^2\int_{\Gamma_{FS}} \upsilon\hat{w}_{\mathbf{n}}\; d\Gamma = \\ = \mathrm{i}\rho\omega\int_{\Gamma_N}\upsilon v_{\mathbf{n}}\; d\Gamma - \sum_r \rho\mathrm{i}\omega q_r\int_\Omega \delta(\boldsymbol{x}_r,\boldsymbol{x})\upsilon\; d\Omega\end{aligned} \tag{25}$$

where υ is the test function, $k = \omega/c$, c is the speed of sound in the fluid, ρ the fluid density, k_i is the wavenumber of the mode i, Ω is the acoustic domain with boundaries: Γ_R (Robin boundary, absorbing with admittance A), Γ_N (Neumann boundary with an imposed velocity $v_{\mathbf{n}}$) and Γ_{FS} the coupling surface with the solid. Point sources at $\boldsymbol{x}_r$ can generate pressure in the acoustic domains.

Considering test functions of the type $\upsilon_i = \mathcal{Y}_n\left(y\right)\psi_i\left(x,z\right)$, each equation i is as follows

$$\begin{aligned}\sum_j p_j\left(\left(k^2-k_i^2\right)I_2\int_{\Omega_{xz}}\psi_i\psi_j\; d\Omega_{xz} - \mathrm{i}\rho\omega I_2\int_{\Gamma_R} A\;\psi_i\psi_j\; d\Gamma_{xz}\right) + \\ +\rho\omega^2 I_{2*}\int_{\Gamma_{FS}}\psi_i\hat{w}_{\mathbf{n}}\; d\Gamma_{xz} = \underbrace{\mathrm{i}\rho\omega I_1\int_{\Gamma_N}\psi_i v_{\mathbf{n}}\; d\Gamma_{xz} - \sum_s \rho\mathrm{i}\omega q_s\mathcal{Y}_n\left(y_s\right)\psi_i\left(x_s,z_s\right)}_{\left(\mathbf{f}_{mod}\right)_i}\end{aligned} \tag{26}$$

with

$$I_1 = \int_{y_{min}=0}^{y_{max}=l_y}\mathcal{Y}_n\left(y\right)\; dy \qquad I_2 = \int_{y_{min}=0}^{y_{max}=l_y}\left(\mathcal{Y}_n\left(y\right)\right)^2\; dy \tag{27}$$

that depend on the interpolation type in the fluid domain and

$$I_{2*} = \int_{y_{min}=0}^{y_{max}=l_y}\sin\left(\frac{n\pi}{L_y}y\right)\mathcal{Y}_n\left(y\right)\; dy \tag{28}$$

that accounts for the fluid-structure coupling. If the function $\mathcal{Y}_n\left(y\right)$ coincides with the equivalent function for the solid element in the extrusion direction, here sine interpolation, then $I_2 \equiv I_{2*}$.

The part in Eq. (26) that needs to be modified due to the coupling with SFEM is the integral on Γ_{FS}. Depending on the orientation of the local coordinate system in the spectral element with respect to the outward normal of the acoustic domain we have (acoustic normal vector pointing outwards)

$$\hat{w}_{\mathbf{n}} = \sigma_s'\hat{w} \tag{29}$$

$\sigma_s' \equiv \sigma_s$ but the prime is used here to distinguish which σ is due to the orientation of the structural displacement with respect to the fluid normal vector pointing outwards when coupling the fluid and the structure in Eq. (29) (this uses σ'), and which one comes from the definition of the structural displacement in Eq. (19) (this uses σ without prime).

The structural displacement $\hat{w}$ of Eq. (6) can be expressed as

$$\hat{w} = \mathbf{N}^{SEM} \cdot \mathbf{A}^T + \frac{1}{D} \sum_{s}^{1\ or\ 2} \sigma_s \sum_{j} \Psi_{s,j} P_{s,j} \cos\left(\kappa_{s,j} x + \varphi_{s,j}\right) \tag{30}$$

and $\mathbf{A}^T$ can be computed from Eq. (19) as

$$\mathbf{A}^T = \mathbf{S}^{-1} \left(\mathbf{u}_e - \frac{1}{D} \sum_{s}^{1\ or\ 2} \sigma_s \sum_{j} \Psi_{s,j} P_{s,j} \mathbf{u}^p_{s,j} \right) \tag{31}$$

Now it can be used to compute $\int_{\Gamma_{FS}} \psi_i \hat{w}_{\mathbf{n}}\ d\Gamma_{xz}$ which in practise implies the computation of the following integrals on the structural element

$$\begin{aligned} \int_{\Gamma_{FS}} \psi_i^{(r)} \hat{w}_{\mathbf{n}}\ d\Gamma_{xz} = & \underbrace{\sigma'_r \int_{\Gamma_{FS}} \psi_i^{(r)} \mathbf{N}^{SEM}\ d\Gamma_{xz} \mathbf{S}^{-1}}_{(\mathbf{C}_{SF})_{i,\cdot}} \mathbf{u}_e \\ & \underbrace{- \sigma'_r \frac{1}{D} \sum_{s}^{1\ or\ 2} \sigma_s \sum_{j} \Psi_{s,j} \int_{\Gamma_{FS}} \psi_i^{(r)} \mathbf{N}^{SEM}\ d\Gamma_{xz} \mathbf{S}^{-1} \mathbf{u}^p_{s,j}}_{(\mathbf{C}^{(r,s)}_{FF})_{i,j}} P_{s,j} \\ & \underbrace{+ \sigma'_r \frac{1}{D} \sum_{s}^{1\ or\ 2} \sigma_s \sum_{j} \Psi_{s,j} \int_{\Gamma_{FS}} \psi_i^{(r)} \cos\left(\kappa_{s,j} x + \varphi_{s,j}\right)\ d\Gamma_{xz}}_{(\mathbf{C}^{(r,s)}_{FF})_{i,j}} P_{s,j} \end{aligned} \tag{32}$$

where the subscript i and superscript r in the mode $\psi_i^{(r)}$ mean that it is the modal function i in the acoustic domain of the side r of the structural element. The same criterion is used for the subscript r in σ'_r which is required due to Eq. (29). $(\mathbf{C}_{SF})_{i,\cdot}$ is a row matrix that couples the mode i with the spectral element, and the coefficient i, j of the matrix $\mathbf{C}^{(r,s)}_{FF}$ couples a mode i of side r with a mode j through the structural element. The modes can be both on the same side of the element or on different sides. For this reason a spectral element with acoustic fluid in only one side needs only one matrix $\mathbf{C}_{FF}$ and when the element is in contact with the fluid on both sides, it implies four matrices $\mathbf{C}_{FF}$: for each side of the element, interaction of the fluid with itself ($\mathbf{C}^{(1,1)}_{FF}$ and $\mathbf{C}^{(2,2)}_{FF}$) and with the fluid on the other side through the forced vibration of the element ($\mathbf{C}^{(1,2)}_{FF}$ and $\mathbf{C}^{(2,1)}_{FF}$). The calculation of the matrix coefficient is done by considering the two indicated integrals in Eq. (32).

The simple problem of two cuboid-shaped acoustic domains (rooms) separated by a single wall (one spectral element), see Fig. 1(b) is considered in order to illustrate the way how the fluid-structure coupling is represented and the organisation of the matrices is done (creation of the coupled system of linear equations). The lower room is denoted by the side number $s = (1)$ and the upper room by the side number $s = (2)$.

It must be also noted that $P_{s,j}$ represents the amplitude of acoustic pressure on the element side. It depends on the value of modal contribution and the evaluation of the mode shape. So, it can be written that

$$P_{s,j} = p_j \cos\left(\frac{n_{zj}\pi}{l_z} z\right) \tag{33}$$

for the lower acoustic domain in Fig. 1(b) $z = l_z$. And $\kappa_{s=1,j} = n_{xj}\pi/l_x$. For the upper acoustic domain, $z = 0$. And $\kappa_{s=2,j} = n_{xj}\pi/l_x$. p_j is the contribution of mode j for the harmonic n_{zj}.

Similar, expressions could be used for the spectral element placed in some of the other three sides of the acoustic domain. The global system of equations is

$$\begin{bmatrix} \mathbf{M_{mod}}^{(1)} + \rho\omega^2 I_2 \mathbf{C}_{FF}^{(1,1)} & \rho\omega^2 I_2 \mathbf{C}_{FF}^{(1,2)} & \rho\omega^2 I_2 \mathbf{C}_{SF}^{(1)} \\ \rho\omega^2 I_2 \mathbf{C}_{FF}^{(2,1)} & \mathbf{M_{mod}}^{(2)} + \rho\omega^2 I_2 \mathbf{C}_{FF}^{(2,2)} & \rho\omega^2 I_2 \mathbf{C}_{SF}^{(2)} \\ \mathbf{C}_{FS}^{(1)} & \mathbf{C}_{FS}^{(2)} & \mathbf{K}_e^{bending} \end{bmatrix} \begin{bmatrix} \mathbf{p}^{(1)} \\ \mathbf{p}^{(2)} \\ \mathbf{u} \end{bmatrix} = \begin{bmatrix} \mathbf{f}_{mod}^{(1)} \\ \mathbf{f}_{mod}^{(2)} \\ \mathbf{f}_{SFEM} \end{bmatrix} \tag{34}$$

with $\mathbf{M_{mod}}$ the modal matrix accounting for the integrals in the first row of Eq. (26), $\mathbf{f}_{mod}$ the modal force vector defined in Eq. (26), $\mathbf{f}_{SFEM}$ the vector of external nodal forces for the spectral element (with the same structure as the nodal force vector defined in Eq. (17)), $\mathbf{p}$ the vector of modal contributions, $\mathbf{u}$ the vector of nodal displacements and rotations. The superscripts indicate the side of the element which is equivalent for this simple case, to the acoustic domain number ((1) for the lower and (2) for the upper).

For more complex structures, the matrices for each structural element and the coupling matrices must be assembled by means of a standard FEM procedure. Note that the size of this linear system of equations is smaller than the dimension of the linear system of equations required by the solution of the same problem by means of a FEM or FSM formulation.

3 Numerical results and analysis

The numerical model is applied to the study of the vibration and sound transmission between two rooms separated by a T-shaped structure (Sections 3.1 and 3.4) or a single wall (Sections 3.2 and 3.3), and four rooms separated by a X-shaped junction (Section 3.5). First, in Section 3.1, the results obtained by means of the modal-spectral model are compared with the results obtained with the finite strip method (FSM) [49]. A single junction (one set of dimensions and material properties) is considered.

Section 3.2 deals with the major numerical drawback of the model. In some situations, $\mathbf{S}$ is very ill-conditioned which causes poor quality of the solutions. It is illustrated with the study of the sound transmission through a single wall. A remedy is also proposed.

In Section 3.4 a parametric analysis to gain knowledge on the general behaviour of the T-junction is performed. It requires a large number of computations and consequently any saving of time is very important. The efficiency is one of the main

advantages of modal-spectral model with respect to other element-based approaches (like FEM or FSM).

Finally, in Section 3.5 the assumption of path independence is checked for an X-junction. The solution of the global problem is compared with the combination of results obtained by simulation of all paths separately.

In all the examples shown here $c = 340$ m/s and $\rho = 1.18$ kg/m^3. The real values of admittance A for the absorbing (Robin) boundaries are taken from Table 1.

$1/A\rho c$	20	32.5	70
$\alpha(\%)$	30	20	10

Table 1: Values of normalised admittance and random incidence absorption coefficient for the Robin boundary condition (calculated as proposed in [50]).

In the T-junction and X-junction cases, each acoustic domain has two rectangular surfaces in contact with the structure, two rectangular surfaces with null pressure ($Y = 0$ and $Y = L_y$) and two rectangular surfaces (Γ_R) where an acoustic absorption can be imposed by means of the admittance value A. The surfaces of null pressure are a consequence of the interpolation functions chosen in the extrusion direction (that are sines, see Eqs. (1) and (24)). Null acoustic intensity passes through them.

In all the simulations the full vibroacoustic problem is solved. It means that in-plane and out-of-plane wave motion in the structure is always possible and fully coupling with all the acoustic domains is considered.

3.1 Comparison with the FSM

As detailed in Section 2, the proposed model has some geometrical limitations: extrusion symmetry and use of sine function as harmonic interpolation in this direction. FSM can exactly reproduce these limitations in order to make a fair comparison. For this reason, the FSM [49] is chosen in order to compare the combination of modal-spectral interpolation with an element-based approach. The treatment of the Y-direction is the same in both models while the difference relies on the $X - Z$ plane. It must be noted that FSM is more flexible in the treatment of the extrusion direction because different interpolation functions in the fluid and the structure can be used without major modifications in the formulation. As detailed above, the proposed model requires equal interpolation functions in the fluid and the solid parts. An additional drawback of FSM with respect to the spectral-modal model is that it still requires the use of a fine discretisation in the two-dimensional plane.

A single T-junction structure that separates a sending and a receiving room is considered. It is made of concrete (see Table 3) with a thickness in each zone of 0.1 m. The total damping $\eta_{total} = \eta_{int} + \eta_{boundary}$ is composed by the internal damping (η_{int}) plus the boundary losses considered with $\eta_{boundary} = f^{-0.5}$ according to [51].

The length of the problem in the extrusion direction is $L_y = 4.0$ m, the sending room has dimensions $L_{x,s} = 3.5$ m $\times L_{z,s} = 2.5$ and the receiving room $L_{x,r} = 4.5$ m $\times L_{z,r} = 2.5$. A point source ($q_s = 0.01$ m^3/s) is placed in bottom left corner of the sending room, separated 0.5 m from the boundaries. More precisely, it is a point

source in the $X-Z$ plane, described by means of a triangular mesh (FSM) or a modal expansion. In the FSM, a node of the triangular mesh is placed in the position of the source which is represented by a non-null term of the force vector corresponding to that node. On the contrary in the modal expansion, the force vector related to each modal contribution is not null. It means that the spatial description of the point source in the $X-Z$ plane, which is of the Dirac delta form, is done through all the modes. Ideally, infinite modes would be required to approximate a Dirac delta function and the truncation of the modal base introduces some additional error in the spatial description of the source. In addition, an element-based interpolation is more adequate than a mode-based to describe the variation of the pressure field around the point source. In the Y-direction, the point sound source requires also the representation of a Dirac delta function. The accuracy depends on the number of harmonics considered. Ideally, infinite sine functions should be required, which is never the case. This number and other model parameters are shown in Table 2 for each third-octave frequency band.

For each frequency f all modes with wavenumber

$$k = \sqrt{\left(\frac{n\pi}{L_y}\right)^2 + \left(\frac{n_{xj}\pi}{l_x}\right)^2 + \left(\frac{n_{zj}\pi}{l_z}\right)^2} \tag{35}$$

in the range $(0,\ 2\pi(\max(1.3f, f+200))/c)$ have been considered. This aspect can be of course optimised, see for example [22, 52]. However, some of the available strategies lose its sense here because solutions are obtained in separate harmonics. This makes in practise not so clear how to neglect the less important modes and keep the efficiency of the implementation. On the contrary, it is an important advantage from the efficiency point of view to split the problem in smaller sub-problems. Each harmonic leads to a linear system of equations with a matrix that is full but has a much smaller dimension than FEM matrices or when the problem is considered as true three-dimensional.

Several transmission paths are taken into account. They are enforced by allowing or not the contact between the structure and the acoustic domains. For example, in the path 13, straight transmission, the sound is generated in the source room which is in contact only with the zone 1 of the T-junction and not with the zone 2. The receiving room is in contact with the zone 3 of the T-junction and not with the zone 2. The model is in the same way adapted to deal with other transmission paths.

Figs. 2 and 3 show pressure levels in each of the rooms

$$L_p = 10\log_{10}\left(\frac{< p_{rms}^2 >}{p_0^2}\right) \tag{36}$$

and velocity levels in each zone of the T-shaped structure

$$L_v = 10\log_{10}\left(\frac{< v_{rms}^2 >}{v_0^2}\right) \tag{37}$$

with the reference values of pressure $p_0 = 2\times10^{-5}$ Pa and velocity $v_0 = 5\times10^{-8}$m/s. $< p_{rms}^2 >$ and $< v_{rms}^2 >$ are respectively the spatial averaged pressure in a room and the spatial averaged velocity in a zone of the structure (the zones are the entire

f_0 (Hz)	num. of harmonics	Δf (Hz)	h_{fluid}	h_{solid}
50	3	1.0	0.4	0.1
63	3	1.0	0.4	0.1
80	4	1.0	0.3	0.1
100	4	2.0	0.3	0.1
125	5	2.0	0.3	0.1
160	6	2.0	0.2	0.1
200	7	2.0	0.2	0.1
250	8	3.0	0.15	0.1
315	10	3.0	0.1	0.1
400	12	4.0	0.1	0.1
500	15	5.0	0.1	0.1
630	18	6.0	0.08	0.1
800	23	10.0	0.06	0.1
1000	28	15.0	0.05	0.1
1250	35	20.0	0.04	0.1

Table 2: Third-octave frequency-band values for several model parameters: f_0 is the central frequency of the band, 'num. of harmonics' is the number of harmonics considered (always starting from 1), Δf is the frequency step or the separation between the considered calculation frequencies, h_{fluid} and h_{solid} are the element sizes used in the fluid and solid part respectively for the FSM cross-sections.

rectangular plates shown in Fig. 1(a)). The nodal points used to make the spatial average are similar in both models and uniformly distributed all around the structure zone or the acoustic domain. The Figs. 2 and 3 are just representative examples of the results obtained for two of the paths.

In both Figs. 2 and 3 the acoustic absorption is 20%. With this value and the mentioned room dimensions, the Schroeder frequency of the rooms is around 350 Hz. The simulations have also been done with acoustic absorption of 10% and 30%, leading to similar conclusions.

The results for all of them show that both models are fully equivalent from the engineering point of view, with the difference that modal-spectral is much faster. This conclusion is valid for all the output types and zones. A difference of 0.4 dB in Fig. 3 is equivalent to a difference of 10% in the spatial averaged output. They are mainly caused by the different discretisation of the point source and treatment of boundaries (absorbing and coupling). In the acoustic domains described by means of the modal expansion, the boundary effects are taken into account through the weak form Eq. (26). This represents just a good approximation but limited by the type of modes used, with null normal derivative at the boundary (for more details see [53]).

The modal behaviour is described in a very similar way for both models in Fig. 2. Only above the 250 Hz the curves start having a small random component without the deeply pronounced peaks due to the resonances. This is coherent with the mentioned value of the Schroeder frequency of the rooms.

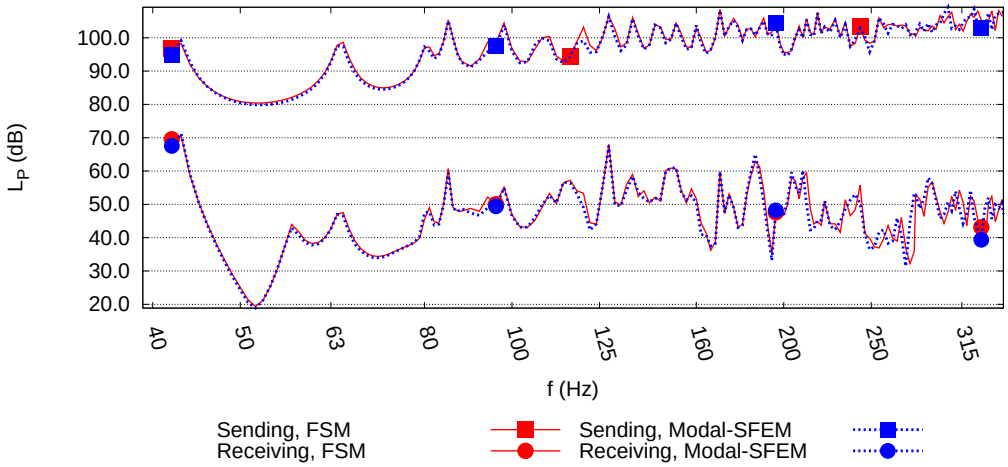

(a)

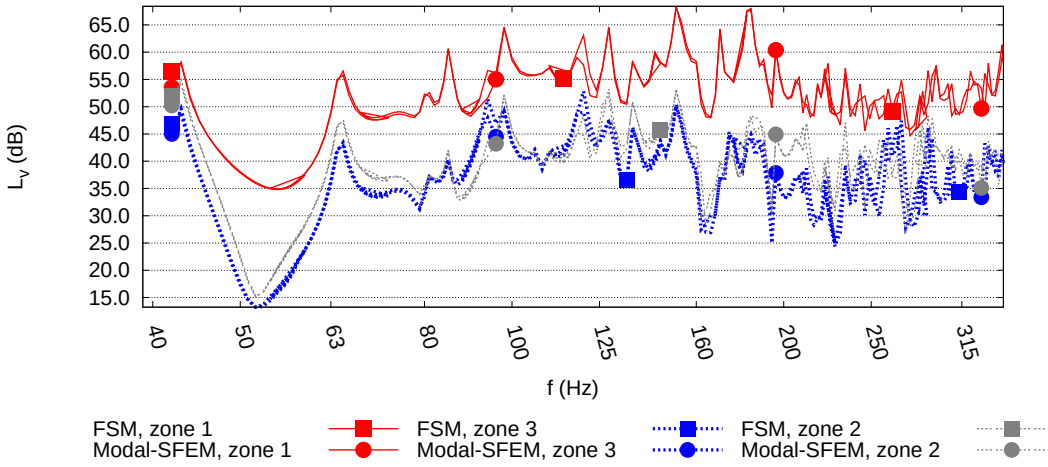

(b)

Figure 2: Example of the frequency-dependent output obtained with the finite strip method (FSM) and the spectral-modal model (Modal-SFEM) with a room absorption of 20%: (a) Pressure levels in sending and receiving rooms for the 12 (right angle) transmission path; (b) Velocity levels for the 13 (straight) transmission path.

3.2 The conditioning problem

The matrix $\mathbf{S}$, for an undamped spectral finite element of length ℓ, is singular if the following equation is satisfied

$$\begin{aligned} 8k_1k_2e^{\mathrm{i}(k_2+k_1)\ell} + \left(\left(k_2^2 - 2k_1k_2 + k_1^2\right)e^{2\mathrm{i}(k_1+k_2)\ell}\right) + \\ +(-k_2^2 - 2k_1k_2 - k_1^2)(e^{2\mathrm{i}k_1\ell} + e^{2\mathrm{i}k_2\ell}) + (k_2^2 - 2k_1k_2 + k_1^2) = 0 \end{aligned} \tag{38}$$

This is a purely numerical phenomenon not related with any physical resonance of the structure. It is important to note that Eq. (38) depends on the physical parameters of the structure but also on the element length. And the element length depends on the discretisation which is independent of the structure dimensions.

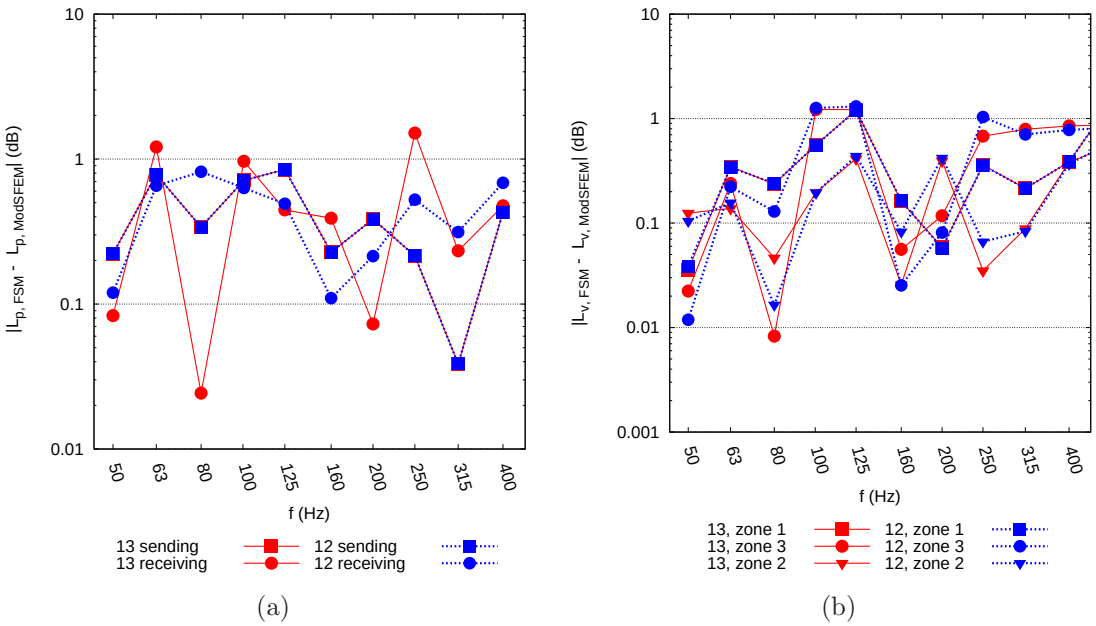

Figure 3: Measure of the differences between the finite strip method and the spectral-modal model. Absolute difference of the third-octave frequency band outputs: (a) pressure levels for several transmission paths; (b) velocity levels for the 13 (straight) transmission path.

The roots of Eq. (38) can be found by successive application of the Newton-Raphson method using different first guesses that cover the whole frequency range of interest. It is not usual to deal with parameters that precisely satisfy this singularity. However, similar situations (lightly damped elements or frequencies that are close to the Eq. (38) roots) can be of interest. In these cases, the matrix $\mathbf{S}^{-1}$ can be very ill-conditioned. See, for example, Fig. 4 that shows the condition number of $\mathbf{S}^{-1}$ for a 0.1 m thick spectral element made of concrete (material properties of Table 3).

The ill-conditioning of $\mathbf{S}^{-1}$ does not affect the performance of the spectral elements for the uncoupled structural problem. However, it can have undesirable consequences for the quality of the numerical solution in the coupled vibroacoustic problem presented here. The propagation of numerical errors is mainly important at low frequencies and for those situations when some spectral element is coupled to the fluid in both sides. It excludes the 12 and 13 transmissions for the T-junction of Section 3.1 but not a simple case of sound transmission through a single wall.

The remedy adopted here in order to overcome this numerical drawback is as follows:

- Make the discretisation of the structure by using the largest spectral elements. In the case of a T-junction, three spectral elements is enough. This saves some computation time.

- Compute all the spurious frequencies as roots of Eq. (38) in all the frequency range of interest and for all the harmonics involved in the solution of the problem.

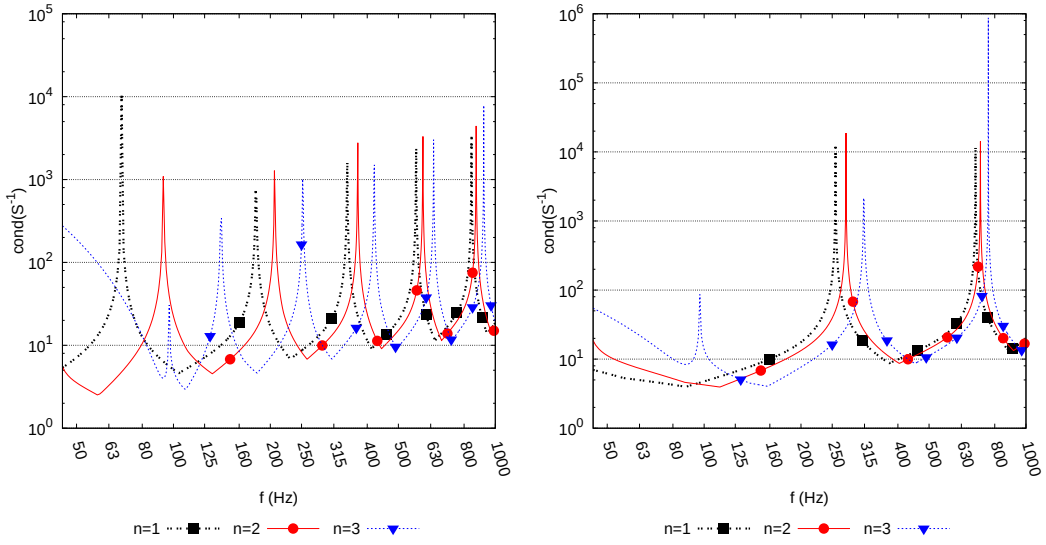

(a) (b)

Figure 4: Condition number of the matrix $\mathbf{S}^{-1}$ for several harmonics n in an spectral element made of concrete: (a) 2.5 m length; (b) 1.25 m length.

- For those situations around the spurious frequencies use an alternative mesh. This mesh can be as simple as divide the problematic spectral element by two. It must be checked that no problems related with the modified discretisation appear around the studied frequency. Fig. 4 shows how the condition number of $\mathbf{S}^{-1}$ varies when modifying the element length. It seems reasonable to define security bands of 10 Hz around the spurious frequencies to activate this remedy (if the calculation frequency falls inside this security band, the probability of obtaining a numerical result affected by the ill-condition problem is important and the remedy is activated). This band can be smaller at high frequencies.

It must be noted that not all the spurious frequencies cause the propagation of numerical errors. But no consistent procedure to determine which of them are problematic has been found.

A model problem is built by considering all the material and geometrical parameters used in Section 3.1 but replacing the T-junction with a single leaf on zone 2. This allows the discussion to be focused in a 2.5 m length element. However, the same comments are valid for the T-junction when the path 33 is analysed or all possible fluid-structure contact surfaces activated. The relevant aspect is to have some of the spectral elements with fluids on both sides.

The results in Fig. 5 illustrate the anomalous behaviour for the sound transmission through a single wall and how the numerical difficulties have been overcome. Three numerical models of the same physical problem are compared: *A)* FSM; *B)* modal-spectral model where the wall is described by means of only one element; *C)* modal-spectral model where the wall is described by means of an alternative discretisation of two elements (1.25 m length each) around the spurious frequencies of model *B*.

Away from the spurious frequencies of the second model (shown by crosses) all the

results are equivalent. However, around the spurious frequencies the results provided by model B largely differ from the FSM prediction. On the contrary, the results provided by model C always agree with the FSM prediction, independently of the studied frequency. The two spurious frequencies around 200 Hz do not affect the quality of the numerical solution.

This is a case where the effect of spurious frequencies is important and affects a quite wide band. In other situations the error peak is more localised around the spurious frequency.

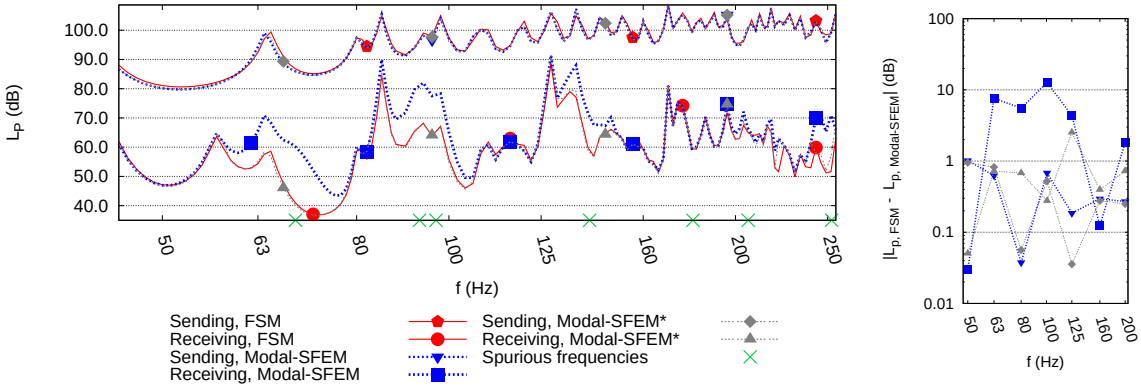

(a) (b)

Figure 5: Effect of the spurious frequencies on the sound transmission through a single wall. The acoustic absorption in both rooms is 20%. The '*' indicates that modal-spectral model uses correction due to ill conditioning (two elements for the wall instead of one). The mean pressure levels in the sending and receiving rooms are shown: (a) frequency-dependent value in each room; (b) difference between FSM and modal-spectral for the third-octave band values.

The ill-conditioning problems caused by the use of 'special' interpolation functions are more important in other numerical techniques: the Wave Based Method [54], the Fundamental Solutions Method [55] and the Partition of Unity Method [56]. Alternatives to the methodology proposed here and based on the scaling of the interpolation functions (especially in the case of evanescent waves), special integration or selective use of wave directions could probably be also derived.

3.3 Influence of boundary conditions in the extrusion direction

As mentioned in Section 2, the model requires sine interpolation in the Y direction. This limits the boundary conditions to be considered at $Y = 0$ and $Y = L_y$. The single wall problem of Section 3.2 is taken as benchmark test in order to study the possible influence of boundary conditions in the acoustic domains.

Sine interpolation is always used for the wall but two options are considered for the acoustic domains: *i)* cosine interpolation which represents that the walls at $Y = 0$ and $Y = L_y$ are rigid (null normal derivative of the acoustic pressure field); *ii)* sine

interpolation that implies the assumption of zero pressure at $Y = 0$ and $Y = L_y$. The first case is solved by means of the FSM [49] and with a fully modal approach where both the acoustic domains and the plate are described by means of a modal expansion as done in [19, 22]. This modal-modal model allows the simulation of higher frequencies than the FSM. For the second case, both models are adapted in order to use sine interpolation in the Y direction. This allows a comparison with the Modal-SFEM model presented here.

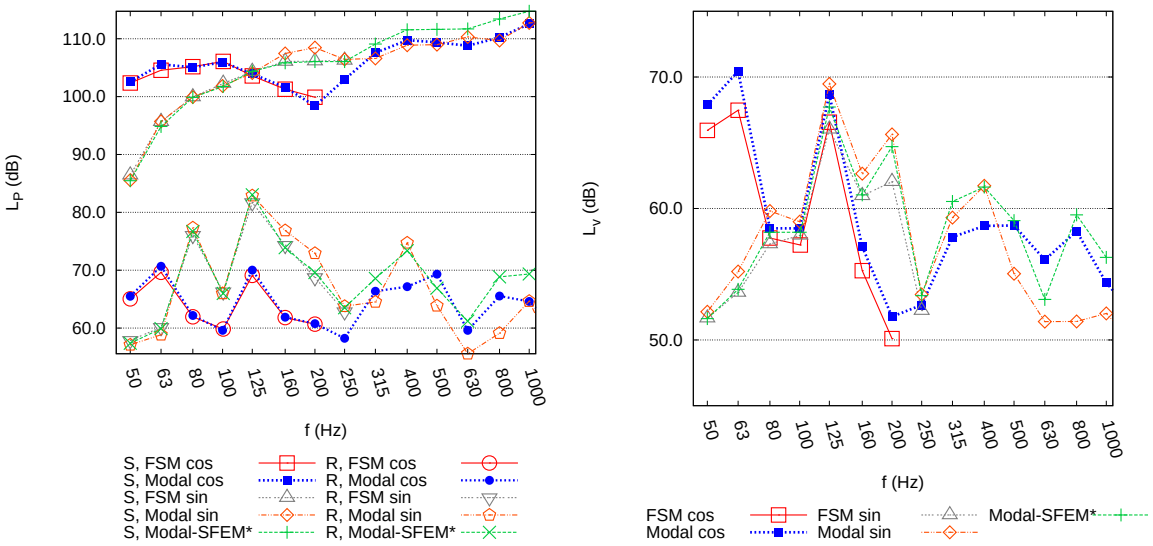

(a) (b)

Figure 6: Sound transmission through a single wall. Influence of boundary conditions, sine or cosine interpolation is used in the Y direction of the acoustic domains. The labels for the models are as follows: 'FSM cos' and 'FSM sin' denote the finite strip method with cosine or sine interpolation in the Y direction respectively; 'Modal cos' and 'Modal sin' is used for the fully modal expansion (acoustic and solid domains) with cosine or sine interpolation in the Y direction respectively; 'Modal-SFEM*' is the Modal-SFEM model presented here with the correction mentioned in Section 3.2. (a)Sound pressure level (The labels 'S' and 'R' mean sending and receiving room respectively); (b) Velocity level.

Fig. 6 illustrates the effect that the modification of the acoustic boundary conditions have on the final outputs. As expected, this is more important at low frequencies. The pressure field of the modes with small $n = 0, 1, 2, \ldots$ is very different (the spatial distribution of pressure in the Y direction differs a lot).

The differences are less important at mid frequencies and larger values of n where even if the pressure field in the Y direction can still be different, the spatial wavenumber is similar and we have different pressure waves that produce a similar excitation on the structure.

3.4 Parametric T-shaped junction

The main advantage of the modal-spectral model is the efficiency. This is illustrated here with the parametric analysis of a T-shaped junction in the framework of a vibroacoustic problem. Recent researches [8, 7, 9] are trying to develop simple but general design rules for the vibration behaviour of some common structural components. A large number of simulations is required in order to make the final prediction formulas independent of the less influencing parameters.

The remainder of the section, is an illustration of how the modal-spectral model can be a useful tool to perform this type of massive vibroacoustic simulations not only at low-frequencies but also at mid-frequencies.

A population of T-junctions is considered. They are generated with the material parameters of Table 3 considering: *i)* homogeneous junctions made of concrete, aerated concrete blocks and calcium silicate blocks; *ii)* junctions made of concrete in the zone 2 and other material in zones 1 and 3 (aerated concrete blocks, bricks or dense aggregate blocks). The thicknesses of each zone can be 0.1, 0.2 and 0.3 m with a total of 9 possible combinations (zones 1 and 3 have always the same thickness). A range of mass ratios according to common junctions found in heavyweight buildings is covered.

The dimensions of the T-junction and rooms are: $L_y = 4.0, 5.0$ or 6.0 m in the extrusion direction, $L_x = 3.5, 4.5$ or 5.5 m and $L_z = 2.5$ m for both sending and receiving rooms. It makes a total of 27 sets of T-junctions and rooms with different dimensions. The result for each junction type (thicknesses and material combination) is provided as the average of these 27 sets of dimensions with the standard deviation. The goal is to obtain a general trend, independent of the problem dimensions.

The main output of interest is the vibration reduction index as defined in [2, 5, 9]

$$K_{ij} = \overline{D_{\nu,ij}} + 10\log_{10}\left(\frac{\ell_{ij}}{\sqrt{a_i a_j}}\right) \quad \text{with} \quad a_i = \frac{2.2\pi S_i}{cT_i}\sqrt{\frac{f_{ref}}{f}} \tag{39}$$

where $\overline{D_{\nu,ij}}$ is the direction averaged vibration level difference, ℓ_{ij} is the length of the junction, a_i is the equivalent absorption length of the plate i, S_i its surface, c the speed of sound in the air, $f_{ref} = 1000$ Hz is a reference frequency and T_i the reverberation time of the wall i that can be calculated as $T_i = 2.2/\left(\eta_{total} f\right)$. $\eta_{total} = \eta_{int} + \eta_{boundary}$ is the total loss factor that accounts for the internal damping (η_{int}) and the boundary losses, considered as $\eta_{boundary} = f^{-0.5}$ according to [51].

For the case of point force excitation, an alternative to compute the spatial average of the velocity level L_v is considered by excluding the zone of 1 m around the point force. This option is indicated in the figures with the symbol '*'. This spatial average tries to neglect the effect caused by the near field around the force application zone and is more coherent with the measurement procedure described in [57].

The coupling surfaces are modified as explained in Section 3.1 in order to allow only one possible transmission path. $K_{i,j}$ is direction averaged. In practise for each junction two situations are considered, sending room on the left and vice-versa. In every situation a point (in the $X - Z$ plane) source is placed in bottom corner, away from zone 2 and separated 0.5 m from the walls. The main difference with previous works[9] is that $K_{i,j}$ is now obtained by means of acoustic excitation instead of point

forces. The effect of the receiving room on the structure can probably be neglected for most of the frequencies if just the $K_{i,j}$ with acoustic excitation needs to be computed. However, at some resonances of the receiving room this hypothesis can be false. It is not easy to determine *a priori* when this can happen. For this reason and thanks to the versatility of the implementation, it is easier and more realistic to consider the receiving room in all the cases.

The mass ratio between the surface density of the orthogonal structural zone and the current one (see [2]) is used as the parameter that characterises the junction.

Material	ρ_v (kg/m^3)	ν	E (Pa)	η_{int}
Concrete	2200	0.2	$3.05 \cdot 10^{10}$	0.005
Aerated concrete blocks (1)	400	0.2	$1.39 \cdot 10^{9}$	0.0125
Aerated concrete blocks (2)	800	0.2	$2.77 \cdot 10^{9}$	0.0125
Dense aggregate blocks	2000	0.2	$1.97 \cdot 10^{10}$	0.01
Bricks	1750	0.2	$1.22 \cdot 10^{10}$	0.01
Calcium silicate blocks	1800	0.2	$1.08 \cdot 10^{10}$	0.01

Table 3: Material properties (frequency independent) of the parametric analysis. Same materials as [8] have been considered.

For each set of 27 junctions, two single values of $K_{i,j}$ are obtained. One is for the low frequencies (average of third-octave frequency bands between 50 Hz and 200 Hz) and the other for mid frequencies (average between 250 Hz and 1000 Hz). The standard deviation of these 27 junctions is also provided. Even if performing single simulations up to 2000 Hz with the mentioned problem dimensions is reasonable, to obtain a high-frequency value (up to 4000 Hz) from a parametric analysis is currently out of the possibilities of the presented model.

The low-frequency results are shown in Fig. 7 for the right-angle transmission (12) and Fig. 8 for the straight transmission (13). Apart from the $K_{i,j}$ values obtained with the vibroacoustic modal-spectral simulations (Modal SFEM), the following data is also plotted: the same $K_{i,j}$ values obtained with the FSM model (for some of the junctions); the $K_{i,j}$ for the same junctions but considering point force excitation (average of three different positions) using the SFEM model described in [9] ,considering spatial average all around the excited plate (SFEM Point Force) or excluding the zone around the force (SFEM Point Force*); the prediction formula proposed in the annex of the EN-12354 regulation [2]; the simplified formula obtained in [8] by statistical regression of a cloud of $K_{i,j}$ data generated by means of a wave approach model (Hopkins).

The predictions done with FSM and modal-spectral are very similar. However, FSM takes much more time. In the low-frequency range, $K_{i,j}$ values obtained with acoustic excitation are in most of the cases 1 or 2 dB larger than their equivalent obtained with point force excitation. However, this trend seems to be inverted for the junctions with the largest mass ratio. In both cases, right angle and straight transmission, the general trend shows the same differences with EN-12354 that are described in [8] or [9]. They are more relevant for the right angle transmission in junctions with a mass ratio different than 1.

The modification in the spatial average of the results obtained with point force excitation causes a reduction of the $K_{i,j}$ values in all cases: low and mid frequencies, straight and right angle transmission. This is explained because the exclusion of the zone around the force application diminished the velocity level in the source plate. The velocity level in the other plates remain the same and consequently the vibration level difference also diminishes. This variation is more important at low frequencies. In the mid frequency range, the values with the modified spatial average are closer to the values obtained with acoustic excitation. This makes sense because the exclusion of the near field produces a more uniform vibration field which is the case of acoustic excitation.

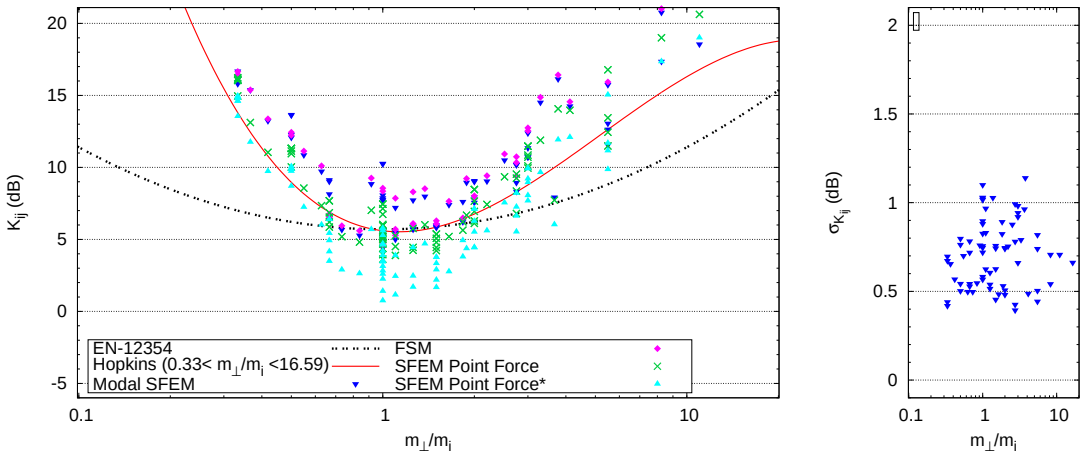

(a) (b)

Figure 7: Low-frequency averaged vibration reduction index for a T-shaped junction, right angle transmission (12): (a) Vibration reduction index for each mass ratio value; (b) Standard deviation of each data point due to the change of junction and room dimensions.

Figs. 9 and 10 are the results for the mid-frequency range. They do not include the FSM data points due to their high computational costs.

The main difference with the low-frequency values is that, now, the $K_{i,j}$ values obtained with acoustic excitation are in most of the cases at least 2 dB smaller than their equivalent obtained with point force excitation (this difference is much smaller if the spatial average excluding the near field is used). With this variation, they are closer to the wave-based prediction formula. This may be caused by the deformation shape at mid frequencies, more affected by damping. When point force excitation is used, damping localises the effect of the force creating a zone around the application point with larger vibration levels. It increases the vibration level of the zone where the point force is applied. If this zone is excluded from the average, the results with acoustic and mechanical excitation are almost equivalent. With acoustic excitation, no local effect is possible and the vibration is more or less uniform (like the excitation is). The standard deviation due to the variation of the junction dimensions is around 1 dB smaller than in the low-frequency range.

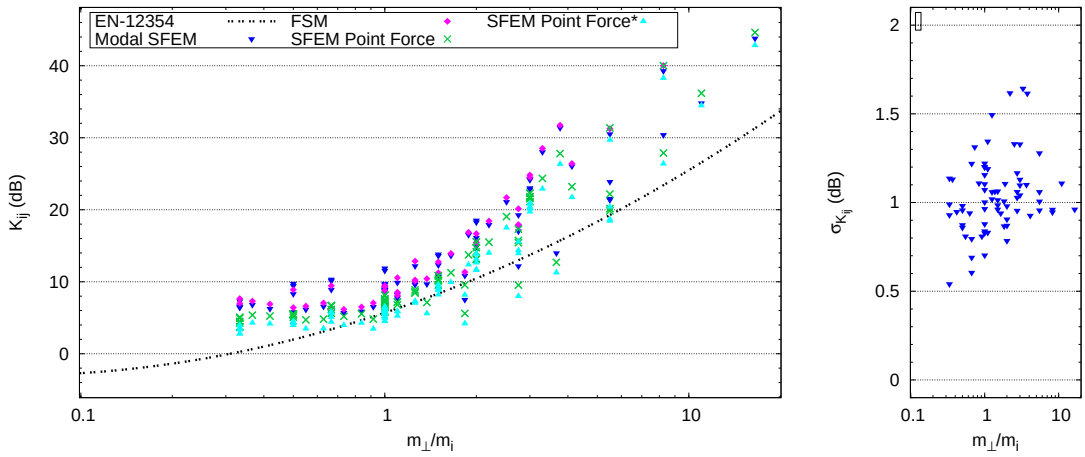

(a) (b)

Figure 8: Low-frequency averaged vibration reduction index for a T-shaped junction, straight transmission: (a) Vibration reduction index for each mass ratio value; (b) Standard deviation of each data point due to the change of junction and room dimensions.

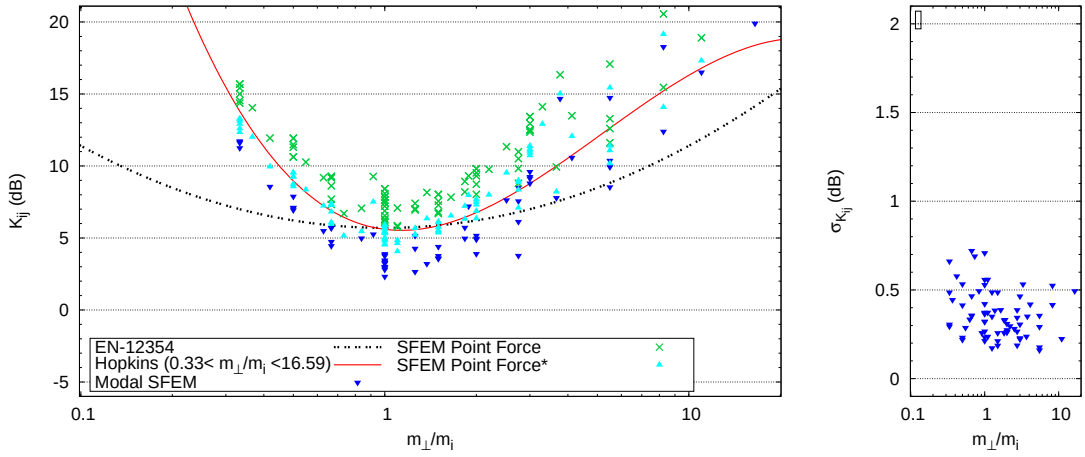

(a) (b)

Figure 9: Mid-frequency averaged vibration reduction index for a T-shaped junction, right angle transmission: (a) Vibration reduction index for each mass ratio value; (b) Standard deviation of each data point due to the change of junction and room dimensions.

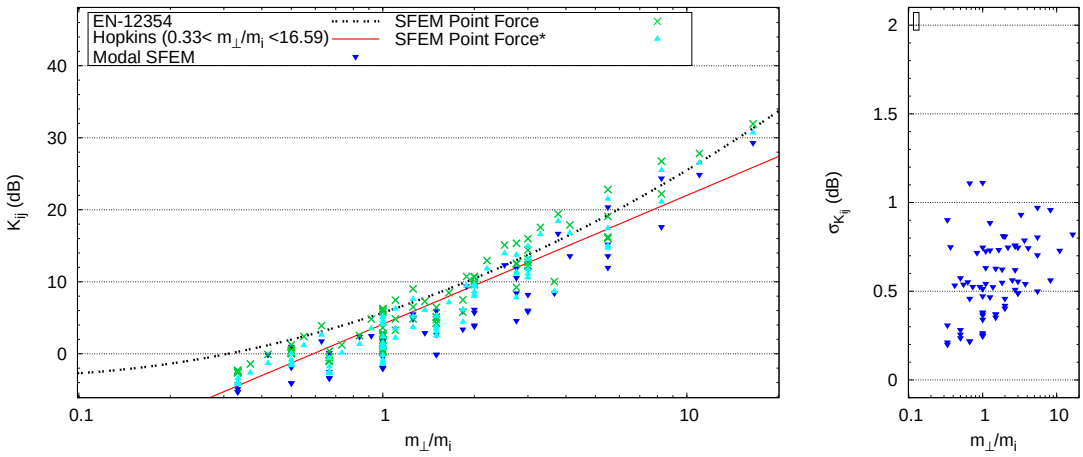

(a) (b)

Figure 10: Mid-frequency averaged vibration reduction index for a T-shaped junction, straight transmission: (a) Vibration reduction index for each mass ratio value; (b) Standard deviation of each data point due to the change of junction and room dimensions.

The largest differences between acoustic and mechanical excitation are found in the low-frequency range. This may be caused, on the one hand, by the less efficient excitation of the vibration field when the acoustic pressure is not a reverberant field [58]. On the other hand, at low frequencies, the vibration response can be dominated by few modes. The coupling efficiency between the excitation and the mode depends on the interaction between the sound waves and the modal shape [59]. This can have a considerable variation from mode to mode and consequently a variability in the vibration levels of the structure.

3.5 Flanking paths superposition

Typical flanking transmissions problems can be solved in a reasonable frequency range by means of the spectral-modal technique. Some of the usual assumptions and simplifications can now be avoided because the fully coupled vibroacoustic formulation of the problem is considered. The fact that the global sound transmission between rooms is modelled by considering independent first-order transmission paths is now verified.

The X-shaped junction of the Fig. 11 is considered. It has the same material properties and dimensions as the T-junction of the Section 3.1 (and $L_{z2} = L_{z4} = 2.5$ m in the upper and lower parts). The reason to chose the X-junction is that while in the T-junction the sound transmission between rooms involves always a direct path, in the X-junction there exist the transmission between the two diagonal (non adjacent) rooms that is done only through flanking (indirect) paths. On the one hand, it makes clearer the role of flanking transmission paths through the structure. On the other hand, it makes easier to check the correctness of the superposition of independent

flanking paths.

For the material and geometrical properties of the junction, the direct path is usually dominant and the effect of one flanking path tends to be marginal. This can be very different in a fully three-dimensional building geometry where the number of indirect paths is increased while the direct path is always one. For example, for a rectangular single wall that separates two rooms and have lateral walls at $Y = 0$ and $Y = L_y$ and upper and lower floors at $Z = 0$ and $Z = L_z$, there are three indirect paths $(1-3,\ 1-2,\ 2-3)$ at each side of the rectangle. It makes a total of twelve indirect paths and only one direct path. This makes clear the potential importance of flanking transmissions in real buildings.

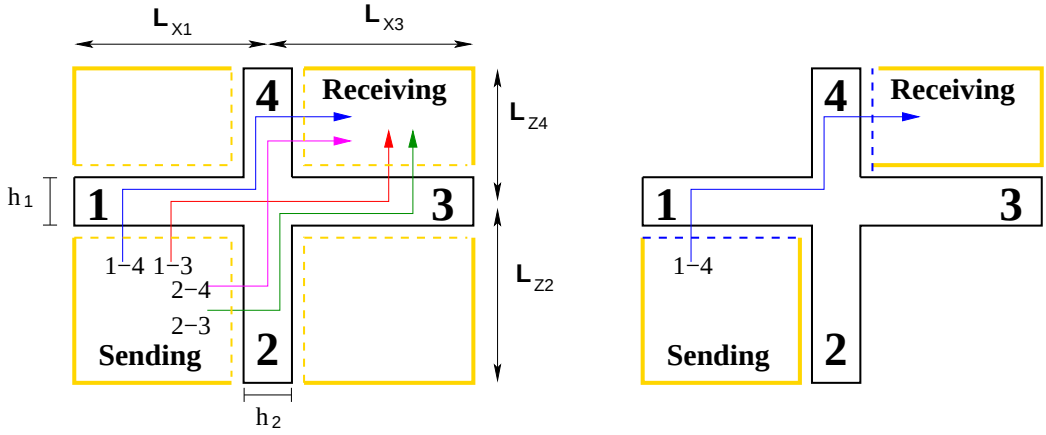

Figure 11: Sketch of a X-shaped junction. On the left, notation used in a situation where all the coupling surfaces are active (dashed lines) and all transmission paths (acoustic and structural) are possible. On the right, problem where the structural transmission path $1-4$ is simulated with only some active coupling surfaces.

The sound reduction index of a flanking path is computed from the numerical simulation as [60, 61]

$$R_{i,j} = L_p^S - L_p^{R,ij} + 10\log_{10}\left(\frac{S_i}{A_R}\right) \tag{40}$$

where L_p^S is the sound pressure level in the sending room, $L_p^{R,ij}$ is the sound pressure level in the receiving room when the transmission path from the zone i to the zone j is allowed, A_R is the total absorbing area in the receiving room and S_i is the area of the structural zone i. When there is direct transmission of sound, S_i is taken as the surface of the wall through which sound is directly transmitted. When there is no direct transmission, like in the case considered here, S_i can be taken as a reference value (10 m^2).

Fig. 12(a) shows the sound reduction indices of the four flanking paths through the diagonal. Apart from the low-frequency zone where the modal behaviour and particular dimensions are important, the general trend of the four paths is very similar. Above the 125 Hz the differences between them are not larger than 8 dB.

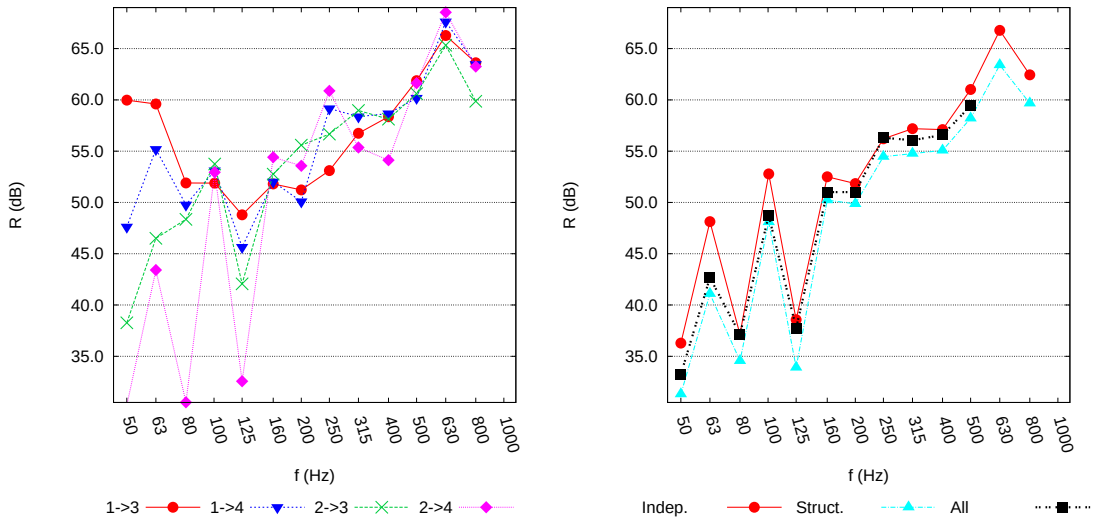

(a) (b)

Figure 12: Flanking transmissions through a X-shaped junction: (a)Sound reduction index (R) of each flanking path through the junction ; (b) Comparison between the overall sound reduction index considering that each indirect flanking path is independent (Indep.), the result when all the structural paths are active at the same time (Struct.), and when all paths (structural and acoustic) are active (All).

The global sound reduction index, taking into account the effect of all the flanking paths is computed as

$$R_{i,j}^{\text{total}} = 10\log_{10}\left(\sum_{i=1}^{N} S_i\right) - 10\log_{10}\left(\sum_{i=1}^{N} S_i 10^{-R_{i,j}/10}\right) \tag{41}$$

where N is the number of paths.

Fig. 12(b) shows the global sound reduction index computed in three different ways: *i)*'Indep.': by superposition according to Eq. (41) of all possible transmission paths, each of them is the result of an individual simulation where the interface conditions between fluid and structure has been properly adapted (see Fig. 11 that illustrates the flanking path $1-4$ with only two coupling surfaces: sending room - zone 1 and receiving room - zone 4); *ii)* 'Struct.': by considering active all possible flanking paths through the X-junction at the same time but not the airborne paths through contiguous rooms (only the sending and receiving rooms are modelled); *iii)*'All': considering the whole problem involving four rooms and all possible transmission paths (acoustic and structural).

A first aspect to be noted is that curves 'Struct.' and 'All' are quite similar. This means that flanking paths through the structure are dominant with respect to the airborne paths between contiguous rooms in the sound transmission through the diagonal. This is not the case in the transmission between adjacent rooms (i.e. in a T-junction) where the airborne (direct) path is clearly dominant. But now, this is a second order path because it needs to pass through two walls (left to right and bottom to top). It drastically penalises the airborne transmission between diagonal rooms.

Except for the low-frequency bands (below 160 Hz), the difference between the 'Struct.' and 'Indep' curves are not very large but it still exists. It means that the superposition of paths is a quite good approximation but not exact. Some interaction between the paths should exist. This observation is based on a meaningful but single example. Most probably a systematic analysis would lead to a more solid conclusion regarding the path superposition.

4 Discussion

The results presented in Section 3 illustrate the potentialities and drawbacks of the proposed model. Section 3.1 shows that it is in practice equivalent to a more versatile method based on polynomial interpolation (i.e. FSM). This is a very positive aspect, which in fact was the main goal of the research. Some of the critical aspects as well as possible improvements and future developments are discussed next.

4.1 Computational efficiency

The formulation of this alternative method makes sense only if the final implementation is more efficient than standard approaches such as FEM or BEM, which is the case. The advantages (in terms of computational cost reduction) of using a modal expansion technique with respect to FEM were studied in [53](Section 5.3) for the case of a single wall modelled with structural FEM elements that separates two cuboid-shaped acoustic domains described by means of a modal expansion, and in [31] for the case of rooms connected through holes, slits or openings. In both cases the advantages of using a modal expansion was clear and expressed in terms of memory requirements, number of degrees of freedom and number of operations. The modal expansion affects to the acoustic part of the problem (rooms) and this advantage is inherited here.

What is improved here is the cost of discretisation of the structure (wall or junction). In [53] it was done by means of finite elements. Even if the use of FEM for the structure is a much smaller penalty than the use of FEM for the rooms, the cost of structural FEM can still be important. Especially if it is compared with the cost of a properly optimised modal description of the rooms. Now, the structural part of the problem is solved with almost marginal costs thanks to the use of spectral elements. For a single wall (one element) it represents eight unknowns (four per node) and for a T-shaped structure three spectral elements and 16 unknowns. And all these is before the elimination of the imposed or blocked displacements. So, it can be said that even if the structural matrices are full in the SFEM the costs associated to the structural part of the problem become almost null.

The matrices lose any specific structure but are very small. The ones associated with the structural part and the coupling are full and those associated with the modal expansion can be diagonal or banded (depending of the treatment of the surfaces with absorption, see the details in [53]). For this reason, a direct solver for full matrices is used here.

The costs associated with the Y direction are equivalent to those described for the FSM in [49]. The convergence analyses presented there, are valid here because the Y

direction is also described by means of trigonometric functions. The most important aspect is the use of the same functions for the structure and acoustic domains that allows the solution of the problem by means of decoupled blocks. This is an important issue from the computational point of view and also from the modelling side (as shown in Section 3.3).

4.2 Weak coupling

Another aspect to be considered is the improvement of the modal expansion used for the acoustic domains with some technique more oriented to the vibroacoustic problems. In the current form, the model is conceived for situations of weak coupling as it is the transmission of sound through walls separating air rooms. This limitation is mainly caused by the use of normal modes (*in vacuo*, see Eq. (23) afterwards) and the lack of normal velocity in the acoustic field but not due to the solution procedure (which is fully coupled). However, this modal expansion is the simplest allowing an analytical treatment of the coupling and has been largely used [62]. Their drawbacks when used for coupled problems (heavy loaded structures or dense fluids) with non-null normal velocity at the fluid boundary are quite well know and some remedies have been proposed. A physical-oriented *a priori* criterion to select the most important modes is used in [52]. A pseudo-static correction of the large numerical errors caused by the truncation of the modal base in strongly coupled problems is proposed in [63]. Another technique that combines a pre-selection of modes and double enrichment of the solutions with information from the coupling forces and final residuals is presented in [64] where an interesting comparison with existing methods is done. The mitigation of truncation errors can also be done in the post-processing stages [65].

The ideas and formulation exposed here could be adapted to account for some of the techniques mentioned above. This could be useful to extend the spectral-modal model presented here to strongly coupled problems (i.e. with heavier fluids). In any of the cases, normal modes are valid for a wide range of situations of interest.

5 Conclusions

The main conclusions of the research are summarised here below:

1. A spectral(structure) and modal (acoustic) model has been developed. The main feature of the formulation is the coupling between both methodologies. The results show a good agreement with the FSM. Moreover, the final model is more efficient (than FSM or three-dimensional FEM) as a result of the combination of more efficient techniques and simplifications of the geometry.

2. Poor quality of the numerical solution around some spurious frequencies is observed. The cause is the ill-conditioning of the matrix $\mathbf{S}$. It is mainly important when some spectral element contacts modal acoustic domains at both sides. This drawback can be overcome by using a slightly different discretisation where the length of the problematic spectral elements is changed.

3. A first application to the study of sound and vibration transmission through a T-junction is done. Some differences in the vibration reduction index computed with point force excitation and with acoustic excitation are observed. They are more important at low frequencies where acoustic excitation systematically provides larger $K_{i,j}$ values. These differences are less important at mid frequencies especially if spatial average that excludes the zone around the point force excitation is considered.

4. The model has also been used to check the hypothesis of flanking path independence. The analysis of a X-shaped junction reveals that some differences between individual path superposition and the global problem exist. They are more important at low frequencies.

A SFEM matrices related with bending

$$\mathbf{S} = \begin{bmatrix} 1 & 1 & e^{-\mathrm{i}k_1 l_x} & e^{-\mathrm{i}k_2 l_x} \\ -\mathrm{i}k_1 & -\mathrm{i}k_2 & \mathrm{i}k_1 e^{-\mathrm{i}k_1 l_x} & \mathrm{i}k_2 e^{-\mathrm{i}k_2 l_x} \\ e^{-\mathrm{i}k_1 l_x} & e^{-\mathrm{i}k_2 l_x} & 1 & 1 \\ -\mathrm{i}k_1 e^{-\mathrm{i}k_1 l_x} & -\mathrm{i}k_2 e^{-\mathrm{i}k_2 l_x} & \mathrm{i}k_1 & \mathrm{i}k_2 \end{bmatrix} \tag{42}$$

$$\frac{\mathbf{B}_e}{D} = \begin{bmatrix} (\gamma_n + k_1^2)\,\mathrm{i}k_1 & (\gamma_n + k_2^2)\,\mathrm{i}k_2 & (-\gamma_n - k_1^2)\,\mathrm{i}k_1 e_1 & (-\gamma_n - k_2^2)\,\mathrm{i}k_2 e_2 \\ \gamma'_n + k_1^2 & \gamma'_n + k_2^2 & (\gamma'_n + k_1^2)\,e_1 & (\gamma'_n + k_2^2)\,e_2 \\ -(\gamma_n + k_1^2)\mathrm{i}k_1 e_1 & -(\gamma_n + k_2^2)\mathrm{i}k_2 e_2 & (\gamma_n + k_1^2)\mathrm{i}k_1 & (\gamma_n + k_2^2)\mathrm{i}k_2 \\ -(\gamma'_n + k_1^2)\,e_1 & -(\gamma'_n + k_2^2)\,e_2 & -(\gamma'_n + k_1^2) & -(\gamma'_n + k_2^2) \end{bmatrix} \tag{43}$$

with $\gamma_n = (2-\nu)\xi_n^2$, $\gamma'_n = \nu\xi_n^2$, $e_1 = e^{-\mathrm{i}k_1 l_x}$ and $e_2 = e^{-\mathrm{i}k_2 l_x}$.

Acknowledgements

Free software has been used [66]. LaCàN research group is grateful for the sponsorship/funding received from Generalitat de Catalunya (Grant number 2014-SGR-1471).

References

[1] S. Schoenwald. *Flanking sound transmission through lightweight framed double leaf walls–Prediction using statistical energy analysis.* PhD thesis, 2008.

[2] EN-12354. Building Acoustics: Estimation of the acoustic performance of buildings from the performance of elements. (Acoustique du bâtiment: Calcul de la performance acustique des bâtiments à partir de la performance des éléments). Technical Report 1–4, 1999-2000.

[3] E. Gerretsen. Calculation of the sound transmission between dwellings by partitions and flanking structures. *Appl. Acoust.*, 12(6):413–433, 1979.

[4] E. Gerretsen. Calculation of airborne and impact sound insulation beteen dwellings. *Appl. Acoust.*, 19(4):245–264, 1986.

[5] Ch. Crispin, B. Ingelaere, M. Van Damme, and D. Wuyts. The vibration reduction index K_{ij}: Laboratory measurements for rigid junctions and for junctions with flexible interlayers. *J. Building Acoustics*, 13(2):99–112, 2006.

[6] Ch. Crispin, M. Mertens, B. Blasco, B. Ingelaere, M. Van Damme, and D. Wuyts. The vibration reduction index K_{ij}:laboratory measurements versus predictions EN 12354-1 (2000). In *The 33rd international congress and exposition on noise control engineering*, Prague, 2004.

[7] Ch. Crispin, L. De Geetere, and B. Ingelaere. Extensions of EN 12354 vibration reduction index expressions by means of FEM calculations. In *Inter-Noise and Noise-con Congress and Conference Proceedings*, volume 249, pages 5859–5868. Institute of Noise Control Engineering, 2014.

[8] C Hopkins. Determination of vibration reduction indices using wave theory for junctions in heavyweight buildings. *Acta Acust. United Acust.*, 100(6):1056–1066, 2014.

[9] J. Poblet-Puig and C. Guigou-Carter. Using spectral finite elements for parametric analysis of the vibration reduction index of heavy junctions oriented to flanking transmissions and EN-12354 prediction method. *Appl. Acoust.*, 99:8–23, 2015.

[10] A. Dijckmans. Structure-borne sound transmission across junctions of finite single and double walls. In *INTER-NOISE and NOISE-CON Congress and Conference Proceedings*, volume 250, pages 2731–2742. Institute of Noise Control Engineering, 2015.

[11] A. Dijckmans. Vibration transmission across junctions of double walls using the wave approach and statistical energy analysis. *Acta Acust. United Acust.*, 102(3):488–502, 2016.

[12] J.F. Doyle. *Wave propagation in structures: spectral analysis using fast discrete fourier transforms*. Springer, New York, 1997.

[13] S. Gopalakrishnan, A. Chakraborty, and D. R. Mahapatra. *Spectral Finite Element Method: Wave Propagation, Diagnostics and Control in Anisotropic and Inhomogeneous Structures*. Springer, 2008.

[14] S. Gopalakrishnan, M. Ruzzene, and S. Hanagud. Spectral finite element method. In *Computational Techniques for Structural Health Monitoring*, pages 177–217. Springer London, 2011.

[15] A. Dijckmans. Modal expansion techniques for predicting sound transmission. In *Proceedings of Inter-Noise 2015*, 2015.

[16] A. Neves e Sousa and B.M. Gibbs. Low frequency impact sound transmission in dwellings through homogeneous concrete floors and floating floors. *Appl. Acoust.*, 72(4):177–189, 2011.

[17] J.T. Du, W.L. Li, H.A. Xu, and Z.G. Liu. Vibro-acoustic analysis of a rectangular cavity bounded by a flexible panel with elastically restrained edges. *J. Acoust. Soc. Am.*, 131(4):2799–2810, 2012.

[18] C. Hopkins, M. Filippoupolitis, and N. Ferreira. Prediction of low-frequency radiation efficiencies using the normal mode approach and finite element methods. In *ICSV22*, Florence, Italy, 2015.

[19] R. Josse and C. Lamure. Transmission du son par une paroi simple. *Acustica*, 14:266–280, 1964.

[20] A.C. Nilsson. Reduction index and boundary conditions for a wall between two rectangular rooms. part i: Theoretical results. *Acta Acust. United Acust.*, 26(1):1–18, 1972.

[21] R.W. Guy and M.C. Bhattacharya. The transmission of sound through a cavity-backed finite plate. *J. Sound Vibr.*, 27(2):207IN7217–216IN8223, 1973.

[22] L. Gagliardini, J. Roland, and J.L. Guyader. The use of a functional basis to calculate acoustic transmission between rooms. *J. Sound Vibr.*, 145(3):457–478, 1991.

[23] W. Kropp, A. Pietrzyk, and T. Kihlman. On the meaning of the sound reduction index at low frequencies. *Acta Acustica*, 2:379–392, 1994.

[24] S. Ljunggren. Air-borne sound insulation of single walls at low frequencies: A discussion on the influence of boundary and mounting conditions. *Building Acoustics*, 8(4):257–267, 2001.

[25] P. Jean and J.F. Rondeau. A simple decoupled modal calculation of sound transmission between volumes. *Acta Acust. United Acust.*, 88(6):924–933, 2002.

[26] T. Bravo and S.J. Elliott. Variability of low frequency sound transmission measurements. *J. Acoust. Soc. Am.*, 115(6):2986–2997, 2004.

[27] E. Reynders. Parametric uncertainty quantification of sound insulation values. *J. Acoust. Soc. Am.*, 135(4):1907–1918, 2014.

[28] P. Davidsson, J. Brunskog, P. Wernberg, G. Sandberg, and P. Hammer. Analysis of sound transmission loss of double-leaf walls in the low-frequency range using the finite element method. *J. Building Acoustics*, 11(4):239–257, 2004.

[29] A. Dijckmans. Wave based modeling of structure-borne sound transmission in finite sized double walls. In *Proceedings of Euronoise 2015*, pages 2531–2536, 2015.

[30] J. Brunskog. The influence of finite cavities on the sound insulation of double-plate structures. *J. Acoust. Soc. Am.*, 117(6):3727–3739, 2005.

[31] J. Poblet-Puig and A. Rodríguez-Ferran. Modal-based prediction of sound transmission through slits and openings between rooms. *J. Sound Vibr.*, 332(5):1265–1287, 2013.

[32] J. Brunskog. Flanking transmission of continuous ground plates. In *Proceeding of Inter–Noise*, 2002.

[33] X. Yu, L. Cheng, and J.-L. Guyader. On the modeling of sound transmission through a mixed separation of flexible structure with an aperture. *J. Acoust. Soc. Am.*, 135(5):2785–2796, 2014.

[34] A. Osipov, P. Mees, and G. Vermeir. Low-frequency airborne sound transmission through single partitions in buildings. *Appl. Acoust.*, 52(3–4):273–288, 1997.

[35] A. Dijckmans, G. Vermeir, and W. Lauriks. Sound transmission through finite lightweight multilayered structures with thin air layers. *J. Acoust. Soc. Am.*, 128(6):3513–3524, 2010.

[36] J. Brunskog and P. Davidsson. Sound transmission of structures. A finite element approach with simplified room description. *Acta Acust. United Acust.*, 90(5):847–857, 2004.

[37] D.A. Bies and C. H. Hansen. *Engineering noise control: theory and practice*. CRC press, 2009.

[38] Y. Naka, A.A. Oberai, and B.G. Shinn-Cunningham. Acoustic eigenvalues of rectangular rooms with arbitrary wall impedances using the interval Newton/generalized bisection method. *J. Acoust. Soc. Am.*, 118(6):3662–3671, 2005.

[39] B. Xu and S. D. Sommerfeldt. A hybrid modal analysis for enclosed sound fields. *J. Acoust. Soc. Am.*, 128(5):2857–2867, 2010.

[40] R.S. Langley. Application of the dynamic stiffness method to the free and forced vibrations of aircraft panels. *J. Sound Vibr.*, 135(2):319–331, 1989.

[41] H. Xu, W.L. Li, and J. Du. Modal analysis of general plate structures. *J. Sound Vibr.*, 136(2):021002, 2014.

[42] M. Boscolo and J.R. Banerjee. Dynamic stiffness elements and their applications for plates using first order shear deformation theory. *Computers & structures*, 89(3):395–410, 2011.

[43] J.R. Banerjee, S.O. Papkov, X. Liu, and D. Kennedy. Dynamic stiffness matrix of a rectangular plate for the general case. *J. Sound Vibr.*, 342:177–199, 2015.

[44] International Organization for Standardization. ISO 140: Acoustics – measurement of sound insulation in buildings and of building elements. Technical report.

[45] R.S. Langley. Analysis of power flow in beams and frameworks using the direct-dynamic stiffness method. *J. Sound Vibr.*, 136(3):439–452, 1990.

[46] A.Y.T. Leung. Dynamic stiffness for structures with distributed deterministic or random loads. *J. Sound Vibr.*, 242(3):377–395, 2001.

[47] F. Birgersson, N.S. Ferguson, and S. Finnveden. Application of the spectral finite element method to turbulent boundary layer induced vibration of plates. *J. Sound Vibr.*, 259(4):873–891, 2003.

[48] F. Birgersson, S. Finnveden, and G Robert. Modelling turbulence-induced vibration of pipes with a spectral finite element method. *J. Sound Vibr.*, 278(4):749–772, 2004.

[49] J. Poblet-Puig and A. Rodríguez-Ferran. The finite strip method for acoustic and vibroacoustic problems. *Journal of Computational Acoustics*, 19(04):353–378, 2011.

[50] P.M.C. Morse and K.U. Ingard. *Theoretical Acoustics*. Princeton University Press, 1968.

[51] R.J.M. Craik. Damping of building structures. *Appl. Acoust.*, 14(5):347–359, 1981.

[52] S. Boily and F. Charron. The vibroacoustic response of a cylindrical shell structure with viscoelastic and poroelastic materials. *Appl. Acoust.*, 58(2):131–152, 1999.

[53] J. Poblet-Puig. *Numerical modelling of sound transmission in lightweight structures*. PhD thesis, 2008.

[54] B. Van Genechten, O. Atak, B. Bergen, E. Deckers, S. Jonckheere, J.S. Lee, A. Maressa, K. Vergote, B. Pluymers, D. Vandepitte, and W. Desmet. An efficient wave based method for solving Helmholtz problems in three-dimensional bounded domains. *Engineering Analysis with Boundary Elements*, 36(1):63–75, 2012.

[55] A.H. Barnett and T. Betcke. Stability and convergence of the method of fundamental solutions for Helmholtz problems on analytic domains. *Journal of Computational Physics*, 227(14):7003–7026, 2008.

[56] R. Hospital-Bravo, J. Sarrate, and P. Díez. Numerical modeling of undersea acoustics using a partition of unity method with plane waves enrichment. *Computational Mechanics*, 57(5):717–732, 2016.

[57] International Organization for Standardization. ISO 10848-1:2006 acoustics – laboratory measurement of the flanking transmission of airborne and impact sound between adjoining rooms – part 1: Frame document. Technical report.

[58] N. Garg and S. Maji. Vibration induced due to acoustic excitation in diffuse field conditions. *Acoust. Aust*, 41:219–224, 2013.

[59] D.C.G. Eaton. An overview of structural acoustics and related high-frequency-vibration activities. *ESA BULLETIN-EUROPEAN SPACE AGENCY*, (92):89–94, 1997.

[60] T.E. Vigran. *Building acoustics*. CRC Press, 2008.

[61] J. Mahn. *Prediction of flanking noise transmission in lightweight building constructions: A theoretical and experimental evaluation of the application of EN12354-1*. PhD thesis, University of Canterbury. Department of Mechanical Engineering, 2009.

[62] C.Q. Howard and B.S. Cazzolato. *Acoustic analyses using Matlab® and Ansys®*. CRC Press, 2014.

[63] M. Tournour and N. Atalla. Pseudostatic corrections for the forced vibroacoustic response of a structure-cavity system. *J. Acoust. Soc. Am.*, 107(5):2379–2386, 2000.

[64] B. B. Smida, R. Majed, N. Bouhaddi, and M. Ouisse. Investigations for a model reduction technique of fluid–structure coupled systems. *Proceedings of the Institution of Mechanical Engineers, Part C: Journal of Mechanical Engineering Science*, page 0954406211411863, 2011.

[65] J. Gu, Z.-D. Ma, and G. M. Hulbert. Quasi-static data recovery for dynamic analyses of structural systems. *Finite elements in analysis and design*, 37(11):825–841, 2001.

[66] C. Geuzaine and J.-F. Remacle. Gmsh: a three-dimensional finite element mesh generator with built-in pre- and post-processing facilities. *Int. J. Numer. Meth. Engng.*, 11(79):1309–1331, 2009.